

Accepted Manuscript

Quasi- static indentation properties of damaged glass/epoxy composite laminates repaired by the application of intra-ply hybrid patches

J. Jefferson Andrew, V. Arumugam, C. Ramesh, S. Poorani, C. Santulli

PII: S0142-9418(17)30205-2

DOI: [10.1016/j.polymertesting.2017.05.014](https://doi.org/10.1016/j.polymertesting.2017.05.014)

Reference: POTE 5020

To appear in: *Polymer Testing*

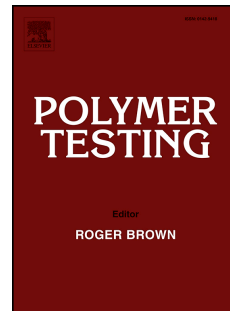
Received Date: 21 February 2017

Revised Date: 11 May 2017

Accepted Date: 11 May 2017

Please cite this article as: J. Jefferson Andrew, V. Arumugam, C. Ramesh, S. Poorani, C. Santulli, Quasi- static indentation properties of damaged glass/epoxy composite laminates repaired by the application of intra-ply hybrid patches, *Polymer Testing* (2017), doi: 10.1016/j.polymertesting.2017.05.014.

This is a PDF file of an unedited manuscript that has been accepted for publication. As a service to our customers we are providing this early version of the manuscript. The manuscript will undergo copyediting, typesetting, and review of the resulting proof before it is published in its final form. Please note that during the production process errors may be discovered which could affect the content, and all legal disclaimers that apply to the journal pertain.



Quasi- Static Indentation Properties of Damaged Glass/Epoxy Composite Laminates Repaired By the Application of Intra-Ply Hybrid Patches

^aJefferson Andrew J, ^aArumugam V, ^{a,*}Ramesh C, ^aPoorani S, ^bC. Santulli,

^aDepartment of Aerospace Engineering, Madras Institute of Technology, Anna University, Chennai, India

^bUniversità degli Studi di Camerino, School of Architecture and Design, Ascoli Piceno, Italy

Abstract:

The main objective of this paper is to investigate the effect of intra-ply hybrid patches based on glass and Kevlar woven fabrics on the local bending response of adhesive bonded external patch repairs in damaged glass/epoxy composite laminates. In intra ply hybrid patches glass and Kevlar fibre reinforcements are combined in the same layer. The intention, in using these hybrid patches, is to combine the excellent mechanical properties of glass fiber as a brittle reinforcement with the superior high elongation to failure property of Kevlar fiber as a ductile reinforcement. Five different kinds of plain weave woven fabrics with different ratios between glass and Kevlar fibers (100/0, 75/25, 50/50, 25/75 and 0/100) were used as the external patches. The undamaged virgin specimens were taken as a reference for the comparison of residual mechanical properties. Multiple quasi-static indentation tests were carried out on repaired glass/epoxy specimens, and their ultimate indentation load, stiffness and permanent deformation were estimated. Failure mechanisms of repaired glass/epoxy specimens under indentation loads were investigated using online Acoustic Emission (AE) monitoring technique. The indentation loads required for the occurrence of various failure modes were measured to illustrate the chronology of progression of different damage modes with increasing load and the kinetics of the various damage modes individually defined in real time. The use of different hybrid patches had a significant effect on the local bending response of the repaired glass/epoxy specimens. In practice, specimens repaired with patches including equal volume fraction of glass and Kevlar fibers presented a more favorable indentation response than virgin ones and other repaired specimens by exhibiting balanced mechanical properties (i.e., high deflection to ultimate failure associated with superior patch-parent laminate bond strength).

Keywords: Polymer composites, Adhesive bonded external patch repair, Multiple quasi-static indentation tests, acoustic emission (AE) monitoring, Hybrid patches.

Introduction

The use of fiber reinforced composite laminates in place of conventional metals is becoming progressively more popular in manufacture of high performance structural components. Composite laminates are materials of first choice for numerous structural applications in aerospace, marine and automobile industries, as they have improved specific mechanical properties, show potential for reparability, are scarcely affected by corrosion, longer fatigue life and are more easily tailored to design requirements. Nowadays, composite laminates

are used for the fabrication of primary load bearing structures of Airbus and Boeing aircraft [1]. These composite laminates are susceptible to low velocity transient impact load. Low velocity impact damage takes place during fabrication or in service or maintenance activities. Low-velocity impact events such as bird strike, tool drops, etc. can induce interlaminar delamination, matrix cracking, and fiber failure and thus reduce the residual strength and stiffness of composite laminates [2]. By low velocity impacts, indentations are typically a sign of sub-surface damage which can comprise of delamination, fiber breakage, and matrix cracks. A significant reduction in tensile and compressive properties is often induced by low velocity impact damage, depending on the impactor diameter, impact number and impact energy. Blunt impacts can encourage sub-surface damage lacking visible exterior damage; it is as a consequence difficult to spot such damage through visual inspections [3]. One of the damage modes that laminated composites will predominantly encounter due to low-velocity impact is interlaminar delamination, which may induce primary or numerous secondary cracks on the composite structure. In conventional metallic structures, impact damage can be evidently observed in the form of an indent. On the other hand, no visible impact damage on the surface may be noted on composites (except glass). Such local damages generally cannot be detected from outside the laminates but they may result in a substantial reduction in structural integrity and load-bearing capacity [4]. Physical damage in laminated composites degrades their mechanical properties and hence reduces their service life. During service life, this local interlaminar delamination may propagate and reduces the stiffness of the structure, leading to premature rupture of the structure below the design level [5]. Moreover, catastrophic premature failure may potentially occur when such laminates are serviced in damaged condition. The mechanical strength and structural integrity of the damaged structural component can be restored either by replacement or repair of the component [6].

The choice of replacement or repair of the damaged component relies on several factors, such as the location of damage on the structure, thickness, aerodynamic requirements, operation conditions (i.e., pressure, temperature and moisture), weight, mechanical property requirements and the damage area or extent of damage [6]. If a damaged structural component is complexly integrated to other structures, repair is the best solution, as the replacement of the whole assembly is very likely not to be economical. Composite laminates are commonly repaired with either adhesive bonded repair technique or mechanical fastener technique. Mechanical fastener repairs on thin composite laminates are not usually preferred as they induce high stress concentration, poor aerodynamic surface and increased overall weight [6]. Presently, the two types of adhesively bonded repair methods utilized to repair a damaged laminate are patch repair and scarf repair. The adhesive bonded scarf repair is usually avoided since it is very difficult to perform, given that the machining process involved in optimum scarfing is time consuming, requires costly equipment and specialized workforce. This repair method is usually applied in cases where flush aerodynamic surface is required and most particularly to repair damaged laminates with thickness exceeding 3 mm [7]. In contrast, adhesive bonded external patch repairs are widely preferred as they are practically easy to perform, compatible to repair thin laminates and consume less time. In addition, adhesively bonded patches have unique advantages over the other repair techniques; like higher residual strength to weight ratio, easy conformance, better fatigue response, corrosion resistance, formability and enhanced service life. Improved damage tolerance of adhesively bonded patches in case of mechanical and environmental loads mean improved safety and superior structural performance in the transportation industry [6]. The mechanical performance of the adhesive bonded repair is influenced by various factors such as

the geometrical parameters, and the type of material considered. Much of the investigation in the area of adhesive bonded external patch repair of composite laminates has been restricted to secondary load bearing structures, highlighting that patch orientation, thickness and geometry and adhesive characteristics (material and thickness) are the major factors influencing the performance of an adhesive bonded patch repair [8-10]. To date, a number of investigations were carried out to optimize patch orientation, thickness and geometry of adhesive bonded external repairs under quasi static in-plane loading conditions using numerical, analytical or experimental approaches. Shiuh and Chao [11] have investigated the effect of patch and adhesive parameters on stress concentration reduction on externally bonded patch repaired composite laminates. They observed that the adhesive parameters have negligible influence on residual mechanical strength of repaired laminates compared to the patch parameters. Liu and Wang [12] studied the influence of different patch lay-up configuration or patch stacking sequence on residual strength of damaged composite laminates repaired using adhesive bonded external patches. They noticed that optimized patch stacking sequence can recover more than 90 % of original strength. They also stated that patch stacking sequence play a major role in structural and operational performance of repair as compared to that of other parameters such as patch thickness, patch shape and adhesive parameters (i.e. adhesive material, adhesive thickness). Furthermore, most of the investigations on adhesively bonded patch repair were performed using unidirectional patches as they offer higher in-plane mechanical properties [4, 20].

On the other hand, unidirectional patches are only suitable for in-plane loading conditions [13-14]. There is considerable attention in tailoring the orientation of adhesively bonded patches so that high performance repaired laminates can withstand in-plane as well as transverse mechanical loadings and can be fabricated. In order to overcome this major drawback it is necessary to develop a patch architecture that enables fabrication of adhesive bonded external patch repairs of minimum thickness and produce post-repaired composite components of residual mechanical strength similar or nearly close to that of normal or virgin components. Intra-ply hybrid patches can be used alternatively to fabricate adhesive bonded external patch repairs of minimum thickness without reducing the residual strength of the repaired laminates. To date, no research work has been done on adhesive bonded external patch repairs in composite laminates using intra-ply hybrid patches. Intra-ply hybrid patches are fabricated using two or more types of fiber reinforcements in a common polymer matrix [15]. They offer a wide range of mechanical properties that cannot be achieved with a single type of fiber reinforcement. Intra-ply hybridization allows modifying the external patch properties to meet the exact needs of the repair under consideration [16]. Particularly, the adhesive bonded intra-ply hybrid external patch repairs can be implemented in areas where the repaired laminates are often subjected to high strain loadings [17]. Even though the significance, range and applications of intra-ply hybridization is further investigated by several researchers, the effects of adhesive bonded intra-ply hybrid external patches on the mechanical behaviour of repaired laminates are not investigated in detail yet. As such, the structural response of these repaired laminates under transverse loading conditions has not been investigated.

In previous research into adhesively bonded patch repair, quasi-static in-plane tensile and compression tests were commonly employed to assess the mechanical performance of adhesively bonded repairs [18-20]. However, information on mechanical behavior during in-plane loading is most likely insufficient to account for the largest number of events during service life of the repaired laminate, therefore it is also important to acquire data on the effect of out-of-plane

loading, of which indentation represents an effective representation. However, when compared to investigations of the mechanical behavior of adhesively bonded patch repairs under in-plane loading conditions, the studies related to out-of-plane loading conditions are limited, even though most of the structural components are subjected to transverse loading. Accordingly, the failure mechanisms and damage propagation at the parent/repair materials interface complicate the structural behaviour of the repaired laminates [21]. Repaired composite structures require regular monitoring to verify their mechanical performance. Monitoring of repaired composites is a rising research area with a potential for online monitoring to inspect critical or subcritical damage in order to improve safety and structural maintenance. For repaired composite structures, a health monitoring set-up could offer opportunities to examine the structural integrity of the repair in real-time (online) and aid schedule condition-based non destructive evaluation. In fiber reinforced composite laminates, the combination of numerous damage modes like fiber/matrix debonding, matrix cracking, delamination and fiber breakage influence the structural integrity of the laminates [22]. The damage in a heterogeneous laminates is indeed developed by an association of numerous micro failure mechanisms [23]. Hence, it is necessary to identify and reckon the individual failure modes to examine the predominance of each failure mode in influencing the ultimate failure of the laminates. The damage mechanisms of these repaired composite laminates are quite complex because of their heterogeneous structure made of the constituent that have appreciably distinct physical and mechanical properties and remain different in a composite structure's final composition. The distinct failure mechanisms and damage propagation behavior of the repaired laminated can alter the structural response of the laminates under mechanical loading. Damage modes such as resin or matrix cracking, fiber/matrix debonding and fiber failure occurring in a lamina do not induce the ultimate collapse of a composite laminate when they occur initially. These damages accumulate progressively within the composite laminates which give rise to the ultimate failure of the specimen [24-25]. Correlation of the different damage profiles with mechanical test results reveal the load to a change in failure mechanisms during mechanical loading concerning the influence of each material system and processing parameters on the performance of repaired glass/epoxy specimens.

Online Acoustic Emission (AE) monitoring is a promising technique which can be employed for in-situ health monitoring or NDE during inspections. Non-destructive techniques (NDTs) such as online Acoustic Emission (AE) monitoring, shearography, ultrasonic, and thermography are frequently used to identify damages modes on laminated composites [22]. Prior to rupture of structures, composite laminates show significant plastic deformation or nonlinear behavior. The dynamic changes induced in the laminates due to mechanical loading cannot be monitored by shearography, ultrasonic, and thermography. Due to ease of real time monitoring of dynamic changes (i.e. damage modes and failure progression) within an anisotropic composite laminate, the Acoustic Emission (AE) monitoring has garnered significant attention in recent times for being considered as a novel non-destructive technique with many advantages than conventional NDT techniques which provides information regarding stagnant defects [23]. Hence, by applying AE monitoring condition-based maintenance rather than scheduled-based maintenance is possible. Furthermore, AE technique enables real time localization of the damage on the structure [24-25].

The main objective of this present work is to investigate the effect of intra-ply hybrid patches based on glass and Kevlar woven fabrics on local bending response of adhesive bonded external patch repairs in damaged glass/epoxy composite laminates under indentation loading. Five different kinds of plain weave woven fabrics with different relative fraction of glass and Kevlar fibers (100/0, 75/25, 50/50, 25/75 and 0/100) were used as the external patches. To investigate the effect of patch hybridization on damage mechanisms and the density of various failure modes of repaired composite laminates, Acoustic Emission (AE) monitoring is conducted in parallel with the mechanical loading.

EXPERIMENTAL PROCEDURE

Materials and fabrication

Plain weave glass fabric of areal density 600 g/m^2 and a LY 556 epoxy resin (supplied by Marktech Composites, India) were used in this study to fabricate the parent composite laminates. Hardener HY 951 was added to the epoxy resin in a ratio of 1:10 by weight as the catalyst to accelerate the curing process. Conventional hand layup technique was employed to reinforce 8 layers of bidirectional glass fiber mats into the epoxy resin in a ratio of 1:1 by weight and cured by the aid of compression molding machine with maximum load capacity 30 kN. The glass/epoxy composite laminates were fabricated into $500 \text{ mm} \times 500 \text{ mm}$ panels with a nominal thickness of $4 \pm 0.1 \text{ mm}$. The hand-laid laminates were cured in the compression mold at ambient temperature under a pressure of 50 kg/cm^2 for about 12 hours. Glass/epoxy indentation specimens of dimension $150 \text{ mm} \times 100 \text{ mm}$ (as per standard ASTM D6264-98) were precisely trimmed from the fabricated laminates using water jet machining process. In order to avoid delamination, the machining was performed at a low water jet pressure of 3400 bar. Subsequently, the machined specimens were carefully inspected for interlaminar delamination before being employed in the repair operation. Since the parent laminate employed in this study was GFRP, visual inspection was appropriate for detecting the presence of delamination failure mode. Totally 24 glass/epoxy specimens were trimmed using this procedure.

Repair Technique

After fabrication, 20 of the 24 specimens were prepared for repair operation. Since external patch repair technique was employed in this study, a through hole of diameter 20 mm was produced in the geometric center of the specimens using an abrasive water-jet cutting machine to induce damage. Moreover, this kind of removal comes about in low velocity impact damage [9]. Before starting with the repair process, the damaged area of the glass/epoxy specimens was wiped using acetone solution to avoid the presence of contaminants and debris from cutting operation (as per standard ASTM D2093) after the water-jet machining process. An epoxy adhesive reinforced with chopped fibers (in a ratio 1:1 by weight) was selected to fill the dressed region, as they showed superior mechanical response to transverse loading [26]. During the repair process, the surplus resin spread around the repair site over the parent laminate was cleaned using cotton immersed in an acetone solution. Bidirectional plain weave square patches with sides of length 60 mm were then externally bonded over the surface of the damaged region of the glass/epoxy specimen. The fiber architecture and the thickness of the individual patches were identical to that of the fabric used to fabricate the parent laminate. Yarn type glass and Kevlar fibers were employed to fabricate intra-ply hybrid patches. Table 1 summarizes

properties of the reinforcements employed in the fabrication of different intra-ply hybrid patches in this study. Five different types of patches were fabricated, a homogeneous Kevlar fabric (100K), a homogeneous glass fabric (100G) and three intra-ply hybrid fabrics, 75G25K, 50G50K and 25G75K, in which the proportion between glass and Kevlar fibers in the warp and fill direction are respectively 75:25, 50:50 and 25:75). Fabrication procedure is indicated in Figure 1 more specifically, four square patches with the quasi-isotropic $([-45, +45]/(0, 90))$ stacking sequences were externally bonded for each side of the repaired specimen. The repaired specimens were allowed curing under a pressure of 50 kg/cm^2 at ambient temperature for about 12 hours using a compression molding machine. Post-curing of all the repaired specimens was performed at 50°C for about 2 hours.

Cyclic quasi static indentation test with AE monitoring

Cyclic quasi static indentation tests were performed in a Tinus Olsen Universal Testing Machine (UTM), equipped with a load cell of maximum load capacity 100 kN, at 0.5 mm/min. Incremental displacement steps of 2, 4, 6, 8, 10 and 12 mm were applied one after the other from the point where the indenter initially contacted (i.e. during 1st indentation cycle) the specimen's surface (including the dent depth). Tests were conducted on both virgin and repair specimens according to the standard ASTM D6264-98. The virgin specimens were used as a reference for comparing the residual strength and mechanical behavior of different repaired specimens. A total of four specimens were tested in each category and the averages of results were considered for interpretation. The rectangular specimens to be tested were firmly fixed on the indentation fixture using toggle clamps (see Figure 2). A hemispherical-faced indenter of diameter 12.7 mm was used to perform cyclic indentation directly above the geometrical center of the repaired region. A Physical Acoustics Corporation (PAC) Acoustic Emission (AE) monitoring device was employed to monitor the real-time dynamic changes within the repaired composite laminates during each cycle of the indentation events. Two wide-band differential AE sensors of operating frequency range 100-900 kHz were used to acquire the stress wave signals generated during fracturing of the repaired specimens under mechanical loading. The distance between the repaired region and either of the two AE transducers was 50 mm. High sealant vacuum grease (silicon grease) was used as the coupling agent between the AE sensor and the repaired glass/epoxy specimens to improve acoustic coupling between them. The AE device was equipped with an eight channel PCI-8 board with a sampling frequency of 4 MHz to simultaneously perform operations such as AE signal acquisition, AE signal processing and high speed transfer of AE data. The acoustic activities and signal parameters were monitored in real-time using AE Win software supplied by PAC. In order to boost the strength of weak acoustic signals for further processing and to reduce the consequence of interference due to external sources, the pre-amplifier gain was set to 40 dB. The amplitude threshold was fixed to 40 dB, which prevents acquisition of unwanted ambient noise signals during damage monitoring process. The wave velocities were mean values estimated as per the standard ASTM E976-10 pencil break test method. The average wave velocity was found to be 3146.3 m/s. The AE events that were recorded by both the sensors were utilized for the data processing.

RESULTS AND DISCUSSION

Mechanical characterization

Figure 3 depicts the variation of indentation force versus indentation displacement for virgin and different repaired composite specimens subjected to multiple quasi static indentation tests. In accordance with the test results, ultimate load of virgin and different repaired specimens are shown in Figure 4. Table 2 summarizes the ultimate displacement and maximum cycles to failure for virgin and different repaired glass/epoxy specimens.

Throughout this paper, the undamaged virgin specimens were taken as the reference for the comparison of residual mechanical properties. The performance of different repair specimens can be ranked by estimating the residual ultimate load. It can be observed that residual ultimate load after repair varies significantly with volume fraction of Kevlar and glass fibers. In particular, the 50G50K specimens show higher ultimate load than the virgin ones, provide the best indentation response. In contrast, the other hybrid and homogeneous laminates all show a decreased ultimate load compared to virgin ones, the highest loss to around 50% of the virgin specimen level was revealed by samples repaired using 100K external patches. Compared to other repaired specimens, in the case of specimens with homogeneous Kevlar patches (i.e. 100 K), the lack of adhesion to the matrix and presence of higher amount of weak hydrogen bond in the transverse direction might have considerably reduced their transverse load carrying capability [27]. These observations were explained further by using damage progression, stiffness progression, residual deflection progression and acoustic emission results from different specimens in the following sections.

Damage propagation, stiffness and permanent deformation observed from the multiple indentation test results of homogeneous and hybrid repaired composite specimens are helpful in the estimation of the balance of various mechanical properties undergone in the repaired specimens due to the influence of hybridization. The permanent deformation is the deflection remaining in the specimen during each cycle of indentation and is a function of indenter's maximum displacement. As a consequence, it cannot be estimated from a monotonic indentation test and therefore the specimens were subjected to multiple quasi-static indentation loads with incremental load steps to perform this evaluation from each force versus displacement curve. The permanent deformation of all the specimens was estimated directly from each load vs. displacement curve, due to the difficulty of reliably mounting an external linear variable differential transformer (LVDT) on the repaired specimens.

Figure 5 depicts the permanent deformation and stiffness for virgin and different repair specimens at various indentation cycles. At 1st indentation cycle, for an indenter maximum displacement of 2 mm, the trend of stiffness was the inverse of the permanent deformation. From Figure 5, for an indenter maximum displacement of 2 mm (i.e., 1st indentation cycle), the virgin specimens showed the least permanent deformation and the highest stiffness. Among repaired specimens, 100G offered the highest stiffness and the minimum permanent deformation. This behavior indicates the brittle nature and lower elongation of the glass fiber. On the other hand, 100K specimens show the least stiffness and maximum permanent deformation, indicating that it withstands the applied indentation load in a ductile manner with higher deflection because of the

higher strain to failure property of the Kevlar fiber. The hybrid repair specimens exhibited a response between 100G and 100K specimens: it was clarified that increasing the volume fraction of Kevlar on the external patches reduces the stiffness of the repair specimens and causes them to withstand the transverse indentation load in a ductile manner.

After a larger number of indentation cycles (i.e., at higher indenter maximum displacement), the permanent deformation also increased. At higher indentation cycles, the virgin, homogeneous and hybrid repair specimens exhibit extremely different responses to indentation load. This evidently highlights the observation that with an increasing indenter maximum displacement, the damage mechanisms responsible for the absorption of applied mechanical energy (i.e. indentation load) are dissimilar. At higher indentation cycles, the 50G50K specimens heavily restrict the damage progression (see photographic images in Figure 6), i.e., specimen with balanced proportion of glass and Kevlar fibers outperforms other hybrid specimens, as observed in stiffness and permanent deformation plot (see Figure 5). In the 2nd indentation cycle, the indenter completely penetrated through the thickness direction of 100G and 75G25K specimens (see Figure 6). A stiffer system would increase the tensile stress on the back face for a given displacement leading to fiber dominated failure. At higher volume fraction of glass fibers in the external patches, the repaired specimens were more rigid; in practice, they exhibited ultimate failure in brittle manner with sudden and catastrophic failure mechanism (i.e., fiber breakage and splitting on the rear face). In addition, virgin specimens also exhibited higher fiber breakage and fiber/matrix debonding, whilst 50G50K specimens, being more flexible, induce damage through high deflection [27]. These observations may explain why virgin, 100G and 75G25K specimens exhibited lower stiffness and higher permanent deformation than 50G50K specimens in the 2nd indentation cycle.

On the other hand, in all indentation cycles, 100K and 25G75K specimens had the maximum permanent deformation and lower stiffness among different specimens (i.e. virgin and various repair specimens). In addition, it can be observed that by increasing the indenter maximum displacement, their permanent deformation and stiffness behavior show abruptly varying trends, indicating that the effect of repair becomes more unpredictable over repeated loading. In the 4th indentation cycle, the difference in permanent deformation and stiffness between 50G50K and virgin specimens were further higher than in 2nd and 3rd indentation cycles, because in this condition, the indenter entirely penetrated the specimen (i.e., predominant fiber breakage of the rear side glass fibers was observed). Even though 100K and 25G75K specimens had higher volume fraction of Kevlar fibers, they revealed ultimate failure at smaller ultimate deflection than 50G50K specimens: this is attributed to the fact that these repair specimens show premature delamination at the parent-patch material interface (see Figure 6). A less stiff system would reduce the stresses at the back face and instead fail with delamination dominated failure at a higher bending displacement.

Quite to the contrary, in the 4th indentation cycle, by reinforcing equal volume fraction of glass and Kevlar fibers into the external patches, the repair specimens (i.e. 50G50K) yielded the best balance between rigidity (high peak load for a displacement of 8 mm), rear face fiber breakage and interlaminar delamination (i.e. superior patch-parent material bond strength). This suggests that for final failure of the specimen, the indentation energy has to increase further, highlighting the superior load carrying capability. Therefore, the maximum deflection to ultimate

failure was significantly higher for the 50G50K rather than the virgin and other repaired specimens. These explanations can be further confirmed by using Acoustic Emission (AE) signatures of different glass/epoxy specimens under multiple quasi-static indentation tests, as elaborated in the following sections.

Acoustic Emission (AE) Characterization:

Unsupervised *k*-means++ analysis of recorded AE events helps in clustering the damage modes generated in the virgin and different repaired specimens, with adequate accuracy [28-29]. The idea is essentially that each damage mode produces an AE event, which is associated in turn to the amplitude of strain energy dissipated as the effect of damage in the specimens. As a result, each AE event has unique characteristics, in the sense that its RMS value, amplitude, counts, duration, frequency and other signal features are related to the failure mechanisms, such as matrix or resin cracking, fiber/matrix debonding, and fiber breakage. The significance of this fact is that different clusters for AE events, associated respectively with matrix or resin cracking, fiber/matrix debonding and fiber breakage can be obtained. AE parameters such as amplitude, duration, energy, counts, rise time, signal strength, absolute energy and RMS value were used as the descriptors to perform the analysis [28-34]. *k*-means++ analysis requires the optimum cluster number “*k*” and the high variance AE descriptors as input entries. Cluster validation parameters, such as Davies–Bouldin index and Silhouette coefficient, were used by many authors to estimate the optimal number of clusters to be opted for the statistical analysis of AE [30-31]. Both Davies–Bouldin index and Silhouette coefficient combine the principle of cohesion and separation to evaluate the optimum cluster number. Davies–Bouldin index evaluates the tightness of data points in each cluster from the proportion of distribution of data points within a particular cluster and the Euclidean distance between the centroid of two nearby clusters. Therefore, the optimal number of clusters should present the lowest value of Davies–Bouldin index, which represents the compactness of data points in a cluster, allows no data points in a cluster similar to other and not excessively short Euclidean distance between the centroids of two clusters. Here, the most favorable value is likely to be less than one [30]. In contrast, Silhouette coefficient measures average Euclidean distance between the data points within a cluster and between two clusters to evaluate how dissimilar each cluster is from any other cluster. Silhouette coefficient (SC) determines how well-separated or dissimilar each cluster is from any other cluster by using average distance between the data points within and between two clusters. Here, the best clusters number should present the highest value of Silhouette coefficient, representing that a data point is compatible to a particular cluster, and incompatible to any other cluster. In this case, the optimal value is expected to be in the range 0.6 to 0.7 according to [30]. Optimum number of clusters (i.e. damage modes) estimated by Davies–Bouldin index and Silhouette coefficient (Table 3) from the recorded acoustic emission events is shown on Figure 7. It can be observed that cluster number *k*=3 were most favorable for clustering the AE data of all the glass/epoxy specimens. The cluster validity evaluations for virgin and different repaired specimens are summarized in Table 3.

In this paper, clustering analysis was carried out with the aid of multivariable principal component analysis (PCA) [32]. PCA helps to visualize and process high-dimensional AE data in an equivalent two dimensional plane (i.e., equivalent 2D new coordinate system with reduced dimensionality). PCA also helps in evaluating the high variance AE descriptors. The percentage

variance and cumulative sum of the variance of each principal component is illustrated in Figure 8. For the whole of glass/epoxy specimens, it was noticed that the cumulative sum of variance of the descriptors amplitude and duration (i.e., first two principal components) provide above 75% of the total variance of the data sets. Since the AE parameters such as amplitude and duration of AE waveform were sufficient to evaluate the failure mechanisms that govern the damage progression of the glass/epoxy composite specimens, the data interpretation is restricted to the first two principal components in the following sections.

Figure 8 illustrates the projection of various clusters by using the first two descriptors or principal components (i.e. amplitude and duration) for all the glass/epoxy specimens. The PCA projection clearly shows that all the clusters were well-separated and the data points within each cluster were well-concentrated. Totally, three well-separated clusters were discriminated during the unsupervised clustering analysis.

Amplitude and duration ranges associated with clusters C_I , C_{II} , and C_{III} are summed up in Figure 9. These distinct ranges can perhaps be related with different failure mechanisms. Generally, it was frequently reported in most of the literature that the AE events with least amplitude and duration correspond to matrix or resin cracking, those with highest amplitude and duration correspond to fiber failure, and those with mid-amplitude and duration ranges relate to delamination or fiber/matrix debonding damage modes [33-34]. Therefore, the pertinent amplitude and duration ranges were: amplitude range 45-61 dB and duration range 0-5611 μ s allied to the matrix or resin cracking, amplitude range 58-78 dB and duration range 0-5940 μ s allied to the fiber/matrix debonding, and amplitude range 78-100 dB and duration range 983-10420 μ s allied to the fiber breakage.

The main step in investigating the multiple indentation behavior of different repaired specimens is to characterize the nature and extent of the damage induced at each indentation cycle. The damage modes corresponding to the clusters C_I , C_{II} , and C_{III} were identified and the correlations between failure location of various damage modes, indentation load, and AE cumulative counts are depicted in Figure 10. The indentation loads required for occurrence of various AE events distributed in these clusters were found to illustrate the chronology of different damage modes with increase of load. In particular, this plot indicates the kinetics of the various damage modes individually in real-time. It can be observed that each consecutive incremental loading step generated more AE events because the indenter maximum displacement increased and consequently damage accumulated. It was also clear that the rate of AE events emitted was maximized when the indenter maximum displacement had almost reached the ultimate value for each indentation cycle. After the peak displacement, the rate of AE event acquisition decreased significantly until up to the next reloading indentation cycle that goes beyond the preceding cyclic ultimate load, as observed in Figure 10.

In general, the failure mode progression mainly depends on the indentation parameters of the test and the material parameters of the specimens. It can be observed in Figure 10 that the nature of damage progressions for virgin, hybrid and homogeneous specimens were entirely different. Figure 11 illustrates the normalized number of overall AE events versus cluster number for virgin and for different repaired glass/epoxy specimens under indentation loading. The similarities of the C_I , C_{II} and C_{III} AE events for different specimens can be better visualized

using the normalized number of overall AE events as a function of different clusters, as some AE events in Figure 10 were overlapped. Fiber/matrix debonding and fiber breakage were the critical failure modes in determining the ultimate load carrying capability of the specimens considered in this study, because the matrix cracking failure mode was recorded almost equal in all the specimens. The dominant damage mechanism leading to ultimate failure with the glass fiber reinforced specimens is fiber breakage, whereas for Kevlar it is fiber/matrix debonding. This behavior evidently highlights that the failure mechanisms responsible for the absorption of applied energy (i.e. indentation load) were different for different specimens.

In the 1st indentation cycle, for a maximum displacement of 2 mm, all the specimens (i.e., virgin and different repaired specimens) responded linearly and emitted no AE events (i.e., no permanent damage). In higher indentation cycles, it can be noticed that the matrix cracking records AE events initially and numerous than other damage modes for all the specimens under indentation load. However, the load corresponding to onset or occurrence of matrix cracking damage mode was different in each specimen. A promising method of evaluating the enhanced structural response of a composite specimen is by estimating the load corresponding to onset of permanent damage (i.e., first AE event or damage initiation). 50G50K repair specimens showed higher indentation load corresponding to the onset of first AE event (i.e., matrix cracking) than the virgin ones, whereas for homogeneous (100G and 100K) and hybrid repair (75G25K and 25G75K) specimens, first AE event occurred at lower load compared to virgin ones. It can be noticed that indentation load for the onset of first AE event was significantly higher for the 50G50K specimens as compared to that for the virgin specimens. 50G50K specimens showed the best structural response to indentation load, as can be also observed in Figures 3-5. Compared to virgin, 100G, 75G25K and 50G50K specimens, in the case of 25G75K and 100 K specimens, the presence of higher permanent deformation (see Figure 5 (a)) might have shifted the initiation of first AE event (i.e., first permanent damage) much more in advance.

In the 2nd indentation cycle, for low Kevlar/glass ratio (Virgin, 100G and 75G25K), the indentation damage zone was concentrated beneath the point of application of indentation load, leading to fiber breakage (see photographic images in Figure 6). Acoustic emission localization plot also depicts that the AE events were predominantly scattered over the center region (i.e. between -20 mm to 20 mm) of the specimens (see Figure 10 (a-c)). In this indentation condition, a significant population of AE events corresponding to fiber breakage was detected. Also, in contrast to gradually increasing cumulative counts of 50G50K, 75G25K and 100K specimens, in specimens with higher amount of glass fiber (i.e. virgin, 100G and 75G25K specimens) significant increment in the cumulative counts occurs from the damage onset region itself. These results can be attributed to the presence of high amount of brittle fibers (i.e. glass fibers). Particularly, in 100G and 75K25G specimens, penetration of the indenter (i.e. ultimate failure) through the thickness, with fiber breakage and splitting on the rear or back face, can be observed (see Figure 6). Damage is generated exactly at the center of these specimens. These results were additional pieces of evidence for sudden and catastrophic brittle fracture mechanism of 100G and 75G25K specimens. Even though penetration was not observed in the 2nd indentation cycle for virgin specimens (see Figure 6), the emission of AE event associate with fiber failure was higher in virgin specimens as compared to 50G50K specimens.

In the 2nd indentation cycle (i.e. for maximum displacement of 4 mm), both 25G75K and 100K specimens showed partial bulge on the rear or tensile side (see Figure 6) as a consequence of high elongation of the Kevlar fibers of outer patches. In these specimens with high volume fraction of Kevlar, no visible fiber breakage was noticed because Kevlar has a high deflection to failure property. By reinforcing more Kevlar fibers into the external patches, the indentation damage extended to a wide area and the AE events were significant in a region between -45 mm to +45 mm (see Figure 10 (e-f)). Precisely, no localized concentration of AE events associated with fiber breakage was found at the center zone as observed for 100G and 75G25K specimens.

In this indentation condition (i.e. in the 2nd indentation cycle), 50G50K repair specimens presented an indentation response more favorable than virgin ones and other repaired specimens (see Figures 10 and 11) because the external patches have been made of equal volume fraction of glass and Kevlar fibers. The Kevlar fibers restrict penetration of indenter and prevent critical fiber breakage (see Figure 6) unlike virgin, 100G and 75G25K specimens, whereas the glass fibers restrict extensive bulge and elongation (see Figure 6) unlike 100K and 25G75K specimens.

Furthermore, in the 3rd indentation cycle (i.e. for maximum displacement of 6 mm), the virgin specimens have a higher amount of fiber breakage AE events than the 50G50K ones (see Figure 10 (a) and (d)). In the 4th indentation cycle, the difference between 50G50K and virgin specimens was considerably higher than in the earlier indentation cycles. For virgin specimens, higher fiber breakage and penetration of the indenter in the 4th indentation cycle were the most dominant factors governing the premature ultimate failure of the specimens as compared to 50G50K repair specimens (see Figure 10 (a) and (d)).

On the other hand, in the 4th indentation cycle, it can be observed that the 25G75K and 100K specimens with higher volume fraction of Kevlar exhibited lower elongation to ultimate failure than 50G50K specimens. Critical fiber/matrix debonding (i.e., delamination) between patch and parent laminate leads to restriction of higher stresses in the farthest tensile fibers (i.e. fibers at the rear patches) to be reached and thus resulting in premature ultimate failure of 25G75K and 100K specimens compared with 50G50K specimens. Photographic images of fractured specimens also depict that the ultimate failure of 25G75K and 100K specimens did not take place by perfect local bending or by predominant breakage of fibers at the rear or tensile side patches of the specimens and no penetration of the indenter to the rear side patches were observed. However, at higher indenter displacement, fiber/matrix debonding (i.e. delamination) of the external patches from the parent laminate was observed (see Figure 6 and Figure 10 (e-f)). Normalized AE event plot also shows that maximum number of AE events corresponding to fiber/matrix debonding (i.e. delamination) damage mode significantly occurred in these specimens (see Figure 11). This evidently explains that the quasi static indentation load was not fully transferred to the tensile side patches during higher deflection, as a consequence of patch-parent laminate delamination. Moreover, from AE results, delamination (i.e. debonding) was the critical failure mode in deciding ultimate failure of 25G75K and 100K specimens repaired using high volume fraction of Kevlar fibers in the external patches as all the other hybrid specimens show ultimate failure due to breakage of fibers at the rear side. This can explain why fiber failure and fiber/matrix debonding was lower in the center zone. This explanation can be further confirmed by using photographic images of damage propagation in these specimens as shown in

Figure 6. In these specimens, fiber/matrix debonding (i.e. delamination) was the dominant damage mode deciding the load carrying capability of the specimens.

From the AE results and the photographic images of failed specimens, it can be concluded that fiber failure was the most important damage mode governing the ultimate failure of specimens with higher amount of glass fiber. On the other hand, parent-patch material interface delamination was the important damage mode deciding the ultimate failure of specimens with higher amount of Kevlar fibers. 50G50K specimens presented an intermediate response between these specimens, although distinct damage patterns were observed as a consequence of the balanced mechanical properties. Among different repaired specimens with higher volume fraction of Kevlar fibers (50G50K, 25G75K and 100K), 50G50K specimens were the only specimens to fail at higher elongation (see Figure 3) with display of significant tensile face fiber breakage (see Figure 6), whereas all other specimens containing Kevlar fibers exhibit parent-patch interface delamination. These results clearly indicate that repaired specimens with higher amount of glass fibers in the external patches have higher stiffness, and also increase the tensile stress on the back face for a given displacement leading to fiber dominated failure (see Figure 11), whereas specimens with higher amount of Kevlar fibers (a less stiff system) would reduce the stresses at this region and instead fail with delamination dominated failure at a higher bending displacement. Additional evidence for this response was that the damage site of fractured specimens with higher amount of glass fibers was almost at the center (see Figure 6). Results indicate that the specimens repaired with equal volume fraction of glass and Kevlar fibers in the external patches presented an indentation response more favorable than virgin ones and other repaired specimens by exhibiting balanced mechanical properties. Acoustic emission results were in accordance with the observations from the permanent deformation and stiffness results, in that the indentation response of the 50G50K was the best under multiple indentation loads.

CONCLUSION

The effects of patch hybridization on multiple quasi-static indentation response of adhesive bonded external patch repaired glass/epoxy composite specimens have been investigated. The experimental results observed from the multiple quasi static indentation tests as well as detailed AE monitoring lead to the following conclusions:

The 50G50K specimens showed higher ultimate load than the virgin ones, while other specimens with hybrid and homogeneous patches exhibited a decreased ultimate load compared to virgin ones.

Also, in terms of permanent deformation and stiffness, 50G50K specimens perform better than virgin ones (except in the 1st indentation cycle), while other homogeneous and hybrid repair specimens show an increased permanent deformation and decreased stiffness compared to virgin ones.

At higher volume fraction of glass fibers in the external patches, the repair specimens were more rigid, so they exhibited ultimate failure in brittle manner with sudden and catastrophic failure mechanism (i.e. fiber breakage and splitting on the rear or back face).

In addition, virgin specimens also exhibit higher fiber breakage, whilst 50G50K specimens, being more flexible, induce damage through high deflection.

In all indentation cycles, 100K and 25G75K specimens had the maximum permanent deformation and lower stiffness among the different specimens (i.e. virgin and various repair specimens).

By reinforcing equal volume fraction of glass and Kevlar fibers into the external patches, the repair specimens (i.e. 50G50K) presented an indentation response more favorable than virgin ones and other repaired specimens. The Kevlar fibers restrict penetration of indenter and prevent critical fiber breakage unlike virgin, 100G and 75G25K specimens, whereas the glass fibers restrict extensive delamination, bulge and elongation unlike 100K and 25G75K specimens.

Acknowledgement:

The author would like to thank Mrs. Jensolin Ebenezer for her inputs in proof reading and editing the document of the manuscript.

Reference:

- [1] Hale J. Boeing787 from the ground up. *Aero Magazine* Boeing 2006; 24 (4):17–23.
- [2] Bhoominathan, R., Vellayaraj, A., Thompson, A. and Andrew Jeyakumar, J. (2015), Residual strength estimation of CFRP laminates subjected to impact at different velocities and temperatures. *Polym. Compos.* doi:10.1002/pc.23796
- [3] Polimeno, U & Meo, M 2009, ‘Detecting barely visible impact damage detection on Aircraft composites structures’, *Composite Structures*, vol. 91, pp. 398–402.
- [4] J. Jefferson Andrew, V. Arumugam, C. Santulli, Effect of post-cure temperature and different reinforcements in adhesive bonded repair for damaged glass/epoxy composites under multiple quasi-static indentation loading, *Composite Structures*, Volume 143, 20 May 2016, Pages 63-74, ISSN 0263-8223, <http://doi.org/10.1016/j.compstruct.2015.10.037>.
- [5] Abrate, S 1991, ‘Impact on laminated composite materials’, *Applied Mechanics Reviews*, vol. 44, no. 4, pp.155–190.
- [6] Whittingham B, Baker AA, Harman A, Bitton D. Micrographic studies on adhesively bonded scarf repairs to thick composite aircraft structure. *Composites: Part A*; 2008.
- [7] Katnam K B, Da Silva L F M, Young T M. Bonded repair of composite aircraft structures: A review of scientific challenges and opportunities *Progress in Aerospace Sciences* 2013; 61: 26–42.
- [8] F. Benyahia, A. Albedah, B. Bachir Bouiadjra. Analysis of the adhesive damage for different patch shapes in bonded composite repair of aircraft structures. *Materials and Design* 2014; 54: 18–24.

- [9] Mohammad Kashfuddoja, Ramji M. Design of optimum patch shape and size for bonded repair on damaged Carbon fibre reinforced polymer panels. *Materials and Design* 2014; 54: 174–183.
- [10] Ouinas D, Bachir Bouiadjra B, Achour T, Benderdouche N. Influence of disbond on notch crack behaviour in single bonded lap joints. *Mater Des* 2010; 31:4356–62.
- [11] Shiuh-Chuan H, Chao MN. Adhesively bonded patch repair of composite laminates. *Adhes Sci Technol* 2011; 25: 2569–85.
- [12] Liu X, Wang G. Progressive failure analysis of bonded composite repairs. *Compos Struct* 2007; 81:331–40.
- [13] F Chen, J M Hodgkinson. Impact behavior of composites with different fiber architecture. *Proceedings of the Institution of Mechanical Engineers, Part G: Journal of Aerospace Engineering*. 223(7): 1009-1017, 2009. DOI - 10.1243/09544100JAERO451. <http://journals.sagepub.com/doi/abs/10.1243/09544100JAERO451>
- [14] George Coppens, Basavaraju Raju, Douglas Templeton. Impact Resistance of Three-dimensional Woven Fabric Composites. American Society for Composites/ American Society for Testing And Materials Committee D30: Nineteenth Technical Conference, October 17-20, 2004. Atlanta, GA.
- [15] Majid Tehrani Dehkordi, Hooshang Nosraty, Mahmood Mehrdad Shokrieh, Giangiacomo Minak, Daniele Ghelli. The influence of hybridization on impact damage behavior and residual compression strength of intraply basalt/nylon hybrid composites. *Materials and Design* 2013; 43: 283–290.
- [16] Majid Tehrani Dehkordi, Hooshang Nosraty, Mahmood Mehrdad Shokrieh, Giangiacomo Minak, Daniele Ghelli. Low velocity impact properties of intra-ply hybrid composites based on basalt and nylon woven fabrics. *Materials and Design* 2010; 31: 3835–3844.
- [17] Akhbari M, Shokrieh MM, Nosraty H. A study on buckling behavior of composite sheet reinforced by hybrid woven fabrics. *Trans CSME* 2008;32:81–9.
- [16] Cheng P, Gong XJ, Hearn D, Aivazzadeh S. Tensile behaviour of patch-repaired CFRP laminates. *Compos Struct* 2011; 93:582–9.
- [18] Pengcheng Cheng, Xiao-Jing Gong, Shahram Aivazzadeh, Xinran Xiao. Experimental observation of tensile behavior of patch repaired composites *Polymer Testing* 34 (2014) 146–154.
- [19] F. Benyahia, A. Albedah, B. Bachir Bouiadjra. Analysis of the adhesive damage for different patch shapes in bonded composite repair of aircraft structures *Materials and Design* 54 (2014) 18–24.

- [20] C. Soutis, D-M. Duan, P. Goutas. Compressive behaviour of CFRP laminates repaired with adhesively bonded external patches *Composite Structures* 1999; 45: 289-301.
- [21] AJ Jefferson, V Arumugam, C Santulli, A Jennifers, M Poorani, Failure Modes of GFRP After Multiple Impacts Determined by Acoustic Emission and Digital Image Correlation, *Journal of Engineering and Technology (JET)*, Volume 6, 31 December 2015, Pages 29-51, ISSN 2180-3811, (<http://journal.utem.edu.my/index.php/jet/article/view/274>).
- [22] RAMESH, C. et al. Effect of Multiple Impacts on GFRP Laminates Exposed to Hydrolytic Ageing using Acoustic Emission Monitoring. *International Journal of Vehicle Structures and Systems*, [S.l.], v. 6, n. 1-2, may. 2014. ISSN 0975-3540. Available at: <<http://maftree.org/eja/index.php/ijvss/article/view/290>>. Date accessed: 18 Apr. 2017. doi:<http://dx.doi.org/10.4273/ijvss.6.1-2.05>.
- [23] Jefferson Andrew, C. Ramesh. Residual strength and damage characterization of unidirectional glass-basalt hybrid/epoxy CAI laminates. *Arabian Journal for Science and Engineering* 2015:2191-4281.
- [24] J. Jefferson Andrew, V. Arumugam, Effect of patch hybridization on the tensile behavior of patch repaired glass/epoxy composite laminates using acoustic emission monitoring, *International Journal of Adhesion and Adhesives*, Volume 74, April 2017, Pages 155-166, ISSN 0143-7496, <http://doi.org/10.1016/j.ijadhadh.2017.01.014>.
- [25] Andrew J, Arumugam V, Sidharth AP, Thomas B. Acoustic emission based monitoring of cut-out geometry effects in carbon/epoxy laminates under uniaxial compression. *International Journal of Vehicle Structures & Systems* 2014; 6:17-23.
- [26] J. Jefferson Andrew, V. Arumugam, K. Saravanakumar, H.N. Dhakal, C. Santulli, Compression after impact strength of repaired GFRP composite laminates under repeated impact loading, *Composite Structures*, Volume 133, 1 December 2015, Pages 911-920, ISSN 0263-8223, <http://doi.org/10.1016/j.compstruct.2015.08.022>.
- [27] AK Vasudevan, RD Doherty *Aluminum Alloys--Contemporary Research and Applications: Contemporary Research and Applications*.
- [28] Arthur D, Vassilvitskii S. K-means++: the advantages of careful seeding. In: *Proceedings of the eighteenth annual ACM-SIAM symposium on discrete algorithms: Society for Industrial and Applied Mathematics*; 2007. p. 1027-35.
- [29] A. Mareca, J. H. Thomasa, R. El Guerjoumaa. Damage characterization of polymer-based composite materials: Multivariable analysis and wavelet transform for clustering acoustic emission data *Mechanical Systems and Signal Processing* 2008; 22: 1441-1464.

- [30] Li Li, Stepan V. Lomov, Xiong Yan, Valter Carvelli. Cluster analysis of acoustic emission signals for 2D and 3D woven glass/epoxy composites. *Composite Structures* 2014; 116: 286–299.
- [31] R. Gutkin, C.J.Green, S.Vangrattanachai, S.T.Pinho, P.Robinson, P.T.Curtis. On acoustic emission for failure investigation in CFRP: Pattern recognition and peak frequency analyses. *Mechanical Systems and Signal Processing* 2011; 25: 1393–1407.
- [32] Jolliffe I. *Principal component analysis*. Wiley Online Library; 2005.
- [33] Andrew JJ, Arumugam V, Bull DJ, Dhakal HN. Residual strength and damage characterization of repaired glass/epoxy composite laminates using AE and DIC. *Composite Structures*. 2016 Sep 15; 152: 124-39.
- [34] Jefferson Andrew, J. and Arumugam, V. (2016), Effect of patch hybridization on the compression behavior of patch repaired glass/epoxy composite laminates using acoustic emission monitoring. *Polym. Compos.* doi:10.1002/pc.24149.

Table captions:

Table 1: Properties of the reinforcements employed in the fabrication of different intra-ply hybrid patches

Table 2: Maximum cycles to failure and ultimate displacement for virgin and different repaired glass/epoxy specimens

Table 3: Cluster validity evaluations for different specimens

Table 1: Properties of the reinforcements employed in the fabrication of different intra-ply hybrid patches

Properties/Fibers	Kevlar	E glass
Tensile strength ($\text{N/m}^2 \times 10^9$)	2.92	3.44
Modulus ($\text{N/m}^2 \times 10^9$)	70.32	72.39
Break elongation %	4.8	3.6
Specific density (kg/m^3)	1439.35	2546.55

Table 2: Maximum cycles to failure and ultimate displacement for virgin and different repaired glass/epoxy specimens

Specimens	Maximum cycles to failure	Maximum Displacement to failure (mm)
Virgin	4	8
100G	2	3.08
75G25K	2	4
50G50K	5	8.84
25G75K	4	7.41
100K	4	8

Table 3: Cluster validity evaluations for different specimens

Specimens	Davies–Bouldin index	Silhouette coefficient
Virgin	0.6795	0.6262
100G	0.7884	0.6327
75G25K	0.69	0.64
50G50K	0.6995	0.5864
25G75K	0.7115	0.6644
100K	0.7811	0.5444

Figure captions

Figure 1 The structure of composite specimens considered in this study: (a) Virgin glass/epoxy specimen, dressed specimens repaired using (b) 100G patches, (c) 75G25K patches, (d) 50G50K patches, (e) 25G75K patches, (f) 100K patches

Figure 2: Glass/epoxy repaired specimen clamped in ASTM D 6264-98 indentation fixture.

Figure 3: Force-displacement curves for (a) Virgin glass/epoxy specimen, dressed glass/epoxy specimens repaired using (b) 100G patches, (c) 75G25K patches, (d) 50G50K patches, (e) 25G75K patches, (f) 100K patches.

Figure 4: Ultimate load of virgin and different repaired glass/epoxy specimens.

Figure 5: (a) Permanent deformation and (b) stiffness progression of virgin and different repaired glass/epoxy specimens.

Figure 6: Photographic images of fractured virgin and different repaired glass/epoxy specimens at various indentation cycles.

Figure 7: Davies–Bouldin index and Silhouette coefficient for (a) Virgin glass/epoxy specimen, dressed glass/epoxy specimens repaired using different patches: (b) 100G, (c) 75G25K, (d) 50G50K, (e) 25G75K, (f) 100K patches.

Figure 8: The variance of principal components and PCA visualization of *k*-means++ clustering for (a) Virgin glass/epoxy specimen, dressed glass/epoxy specimens repaired using (b) 100G patches, (c) 75G25K patches, (d) 50G50K patches, (e) 25G75K patches, (f) 100K patches.

Figure 9: The summary of the failure mode discrimination using amplitude and duration ranges.

Figure 10: Indentation load, AE cumulative counts and AE event location versus time for (a) Virgin glass/epoxy specimen; dressed glass/epoxy specimens repaired using (b) 100G patches, (c) 75G25K patches, (d) 50G50K patches, (e) 25G75K patches, (f) 100K patches.

Figure 11: Normalized number of AE events (%) versus clusters for virgin and different repaired glass/epoxy specimens.

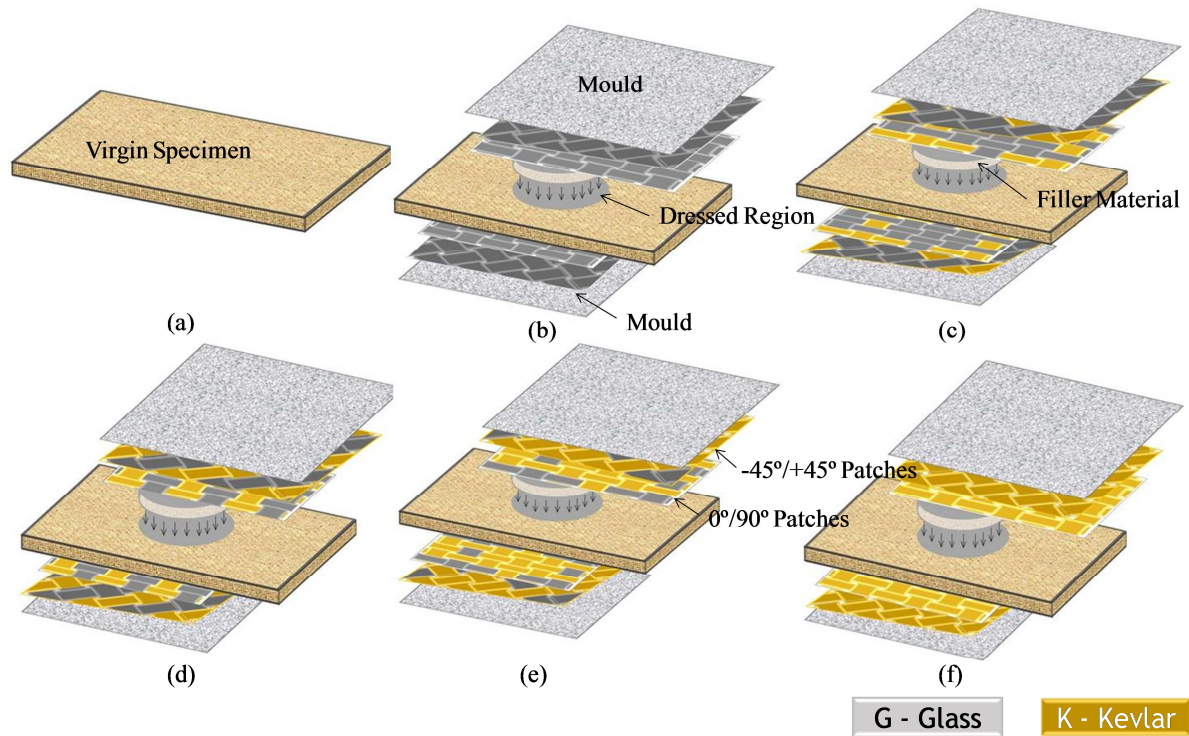
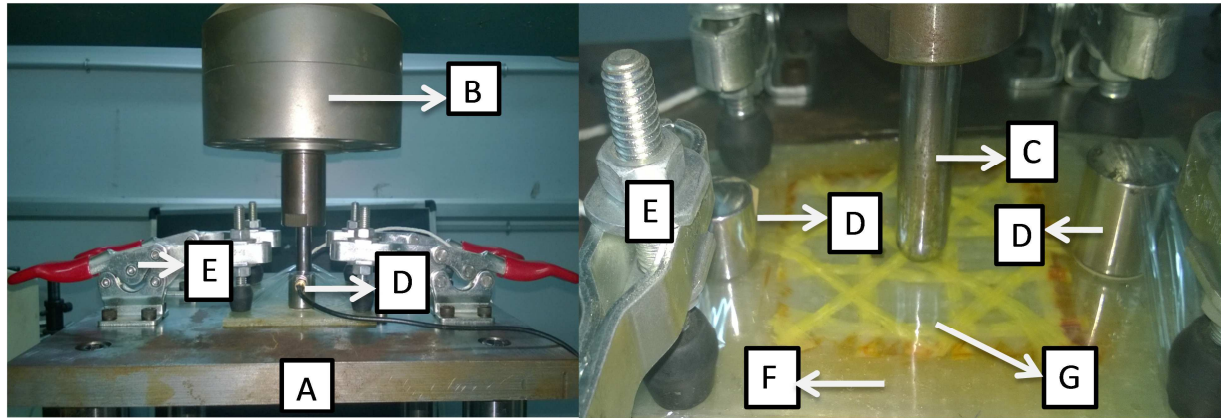


Figure 1 The structure of composite specimens considered in this study: (a) Virgin glass/epoxy specimen, dressed specimens repaired using (b) 100G patches, (c) 75G25K patches, (d) 50G50K patches, (e) 25G75K patches, (f) 100K patches



A - ASTM D6264-98 Indentation Fixture **B** – 100 kN Load Cell **C** – Indenter **D** – AE Sensor,
E - Toggle Clamps **F** - GFRP Repaired Specimen **G** – Repaired Area

Figure 2: Glass/epoxy repaired specimen clamped in ASTM D 6264-98 indentation fixture.

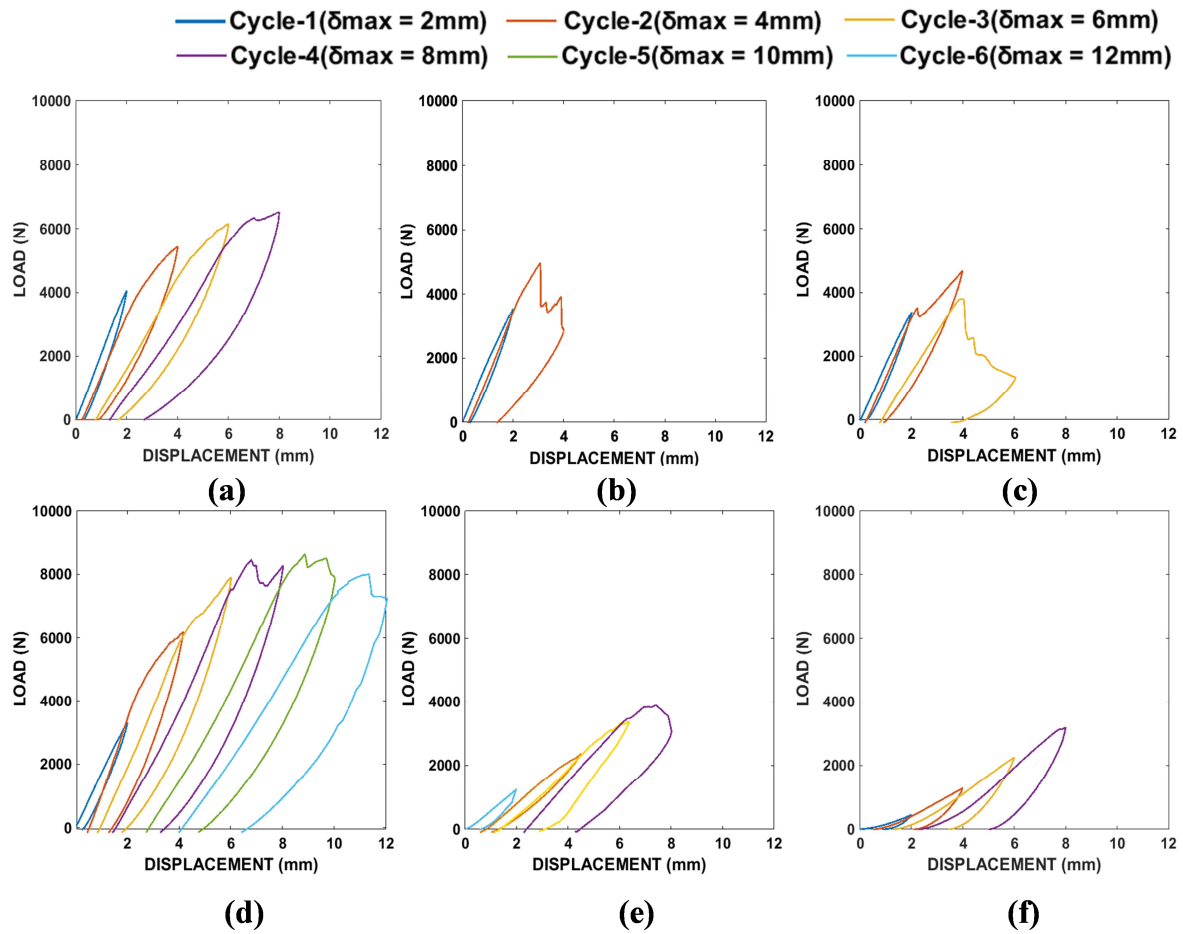


Figure 3: Force-displacement curves for (a) Virgin glass/epoxy specimen, dressed glass/epoxy specimens repaired using (b) 100G patches, (c) 75G25K patches, (d) 50G50K patches, (e) 25G75K patches, (f) 100K patches.

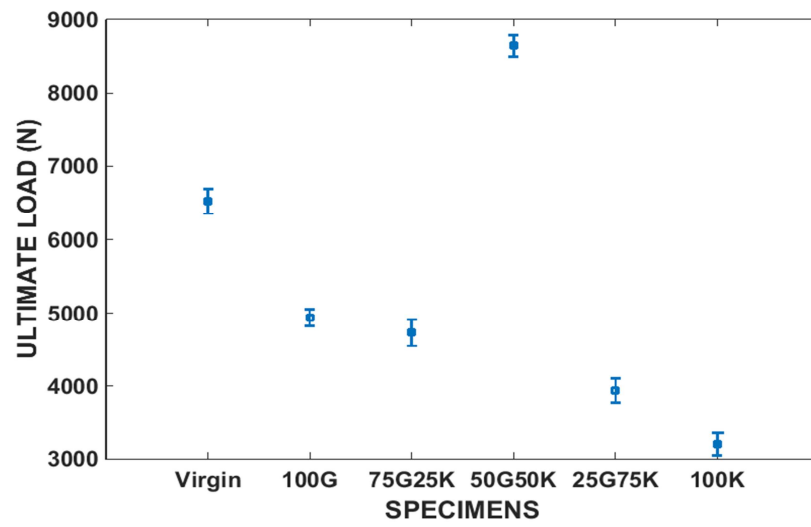


Figure 4: Ultimate load of virgin and different repaired glass/epoxy specimens.

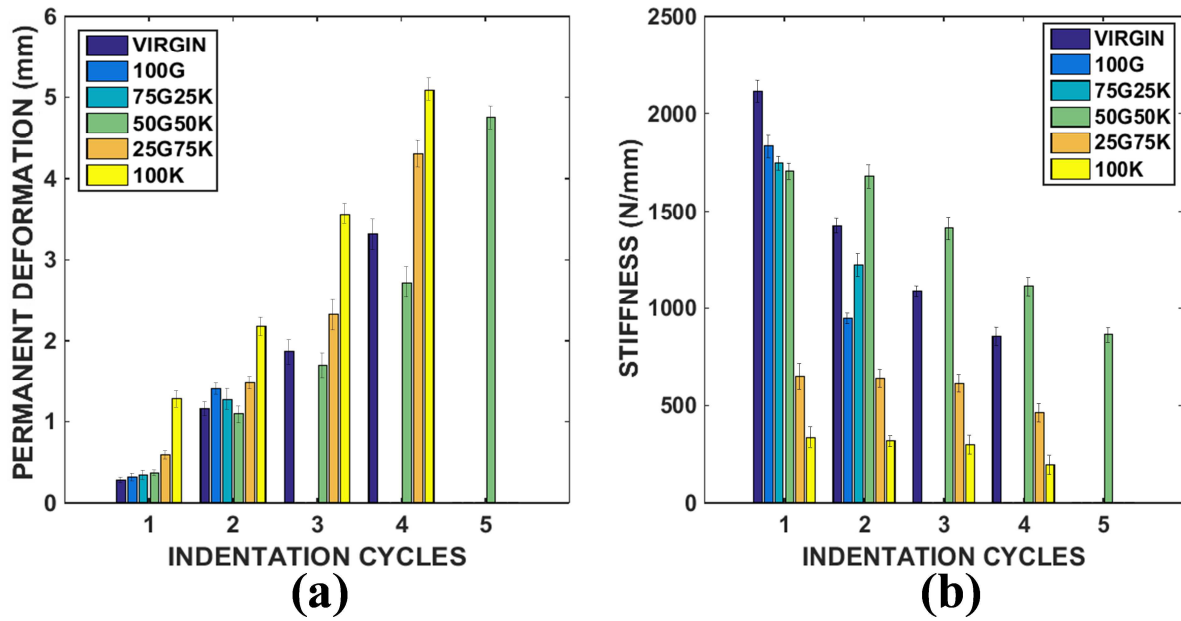


Figure 5: (a) Permanent deformation and (b) stiffness progression of virgin and different repaired glass/epoxy specimens.

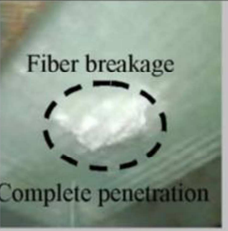
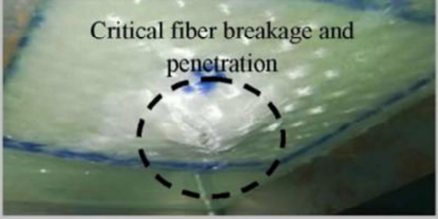
VIRGIN					
	P=4070 N, D=2 mm	P= 5423 N, D=4 mm	P=6150 N, D=6 mm	P= 6520 N, D=8 mm	
100G					
	P=3550 N, D=2 mm		P=4940 N, D=3.08 mm		
75G25K					
	P=3450 N, D=2 mm		P=4730 N, D=4 mm		
50G50K					
	P=3310 N, D=2 mm	P= 6240 N, D=4 mm	P=7940 N, D=6 mm	P= 8480 N, D=8 mm	P=8640 N, D=8.8mm

Figure 6: Photographic images of fractured virgin and different repaired glass/epoxy specimens at various indentation cycles.

25G75K		 Rear side bulging leading to delamination	 Extensive bulging- widespread delamination Minor fiber breakage	 Complete parent-patch delamination
	P=1240 N, D=2 mm	P= 2430 N, D=4 mm	P=3440 N, D=6 mm	P= 3940 N, D=7.41 mm
100K		 Rear side bulging- delamination initiation	 Extensive bulging- widespread delamination Minor fiber breakage	 Extensive delamination
	P=448 N, D=2 mm	P= 1280 N, D=4 mm	P=2260 N, D=6 mm	P= 3200 N, D=8 mm

Figure 6: (Continued)

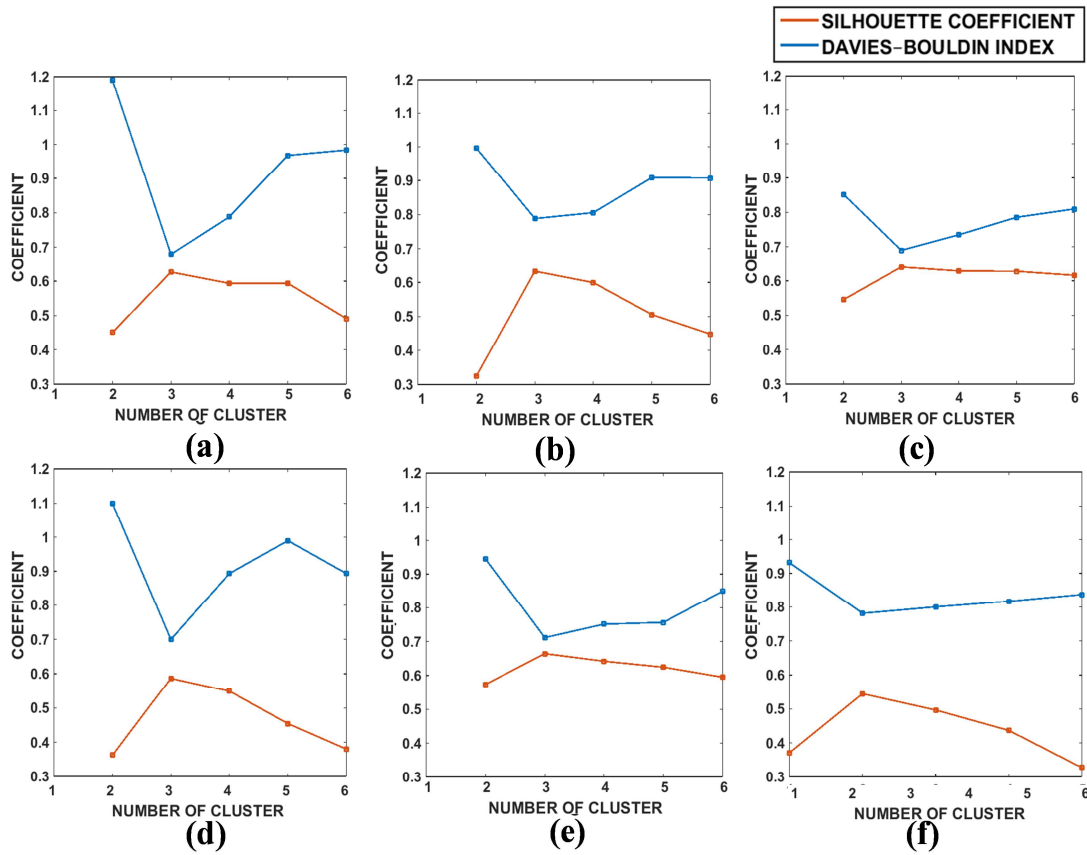


Figure 7: Davies–Bouldin index and Silhouette coefficient for (a) Virgin glass/epoxy specimen, dressed glass/epoxy specimens repaired using different patches: (b) 100G, (c) 75G25K, (d) 50G50K, (e) 25G75K, (f) 100K patches.

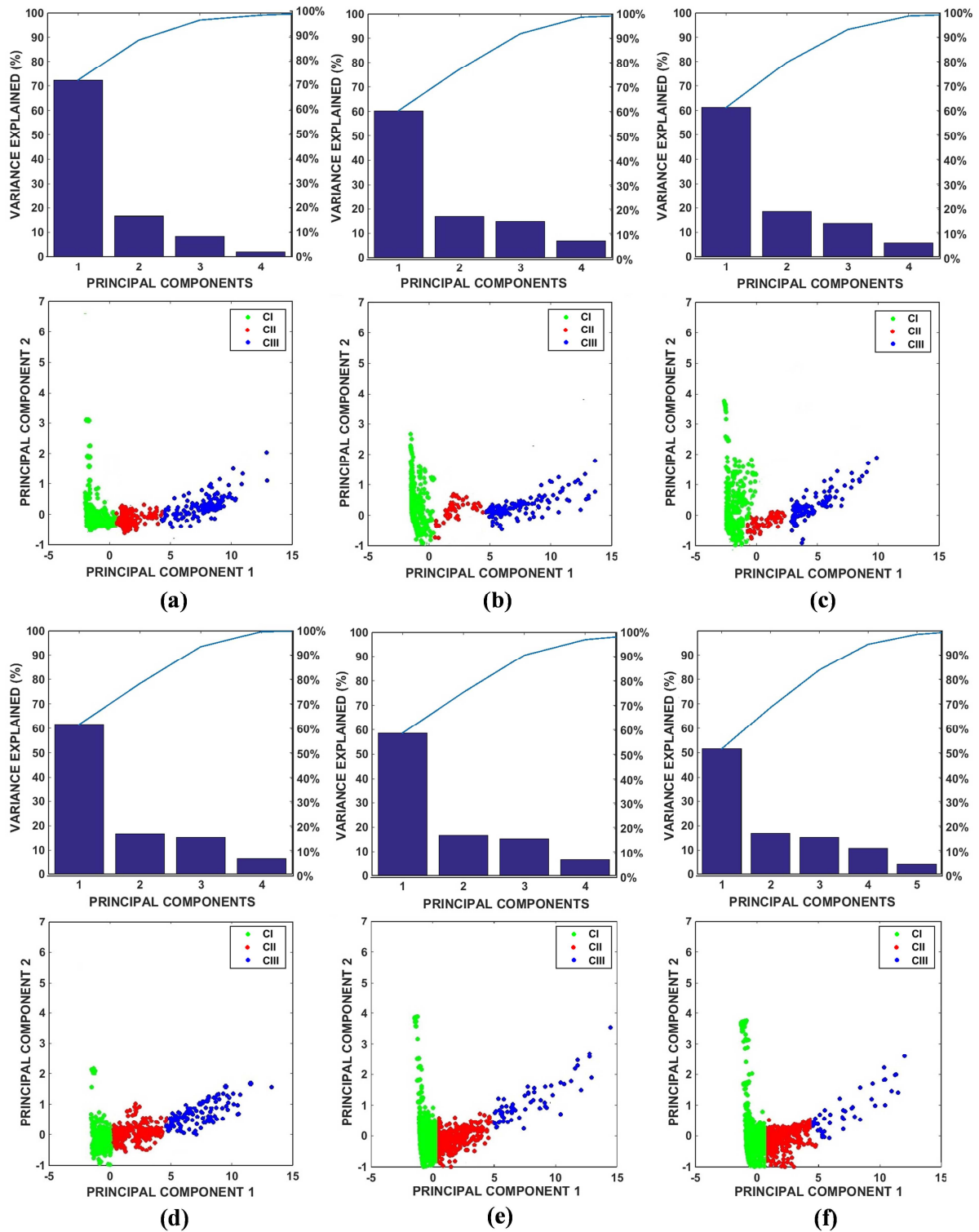


Figure 8: The variance of principal components and PCA visualization of *k*-means++ clustering for (a) Virgin glass/epoxy specimen, dressed glass/epoxy specimens repaired using (b) 100G patches, (c) 75G25K patches, (d) 50G50K patches, (e) 25G75K patches, (f) 100K patches.

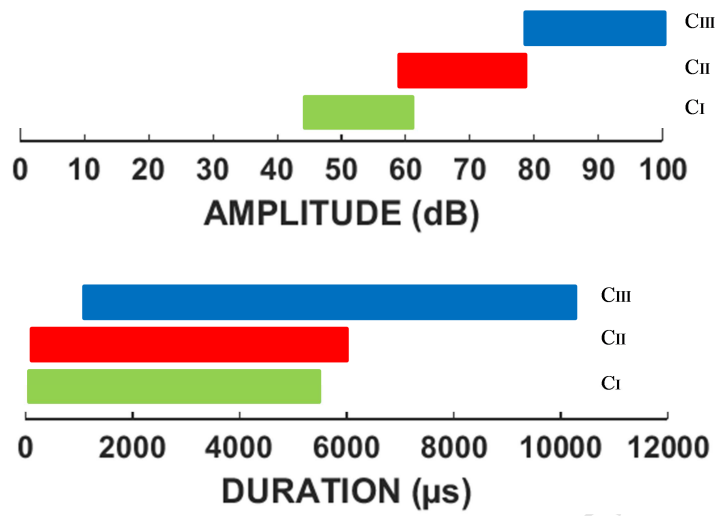


Figure 9: The summary of the failure mode discrimination using amplitude and duration ranges.

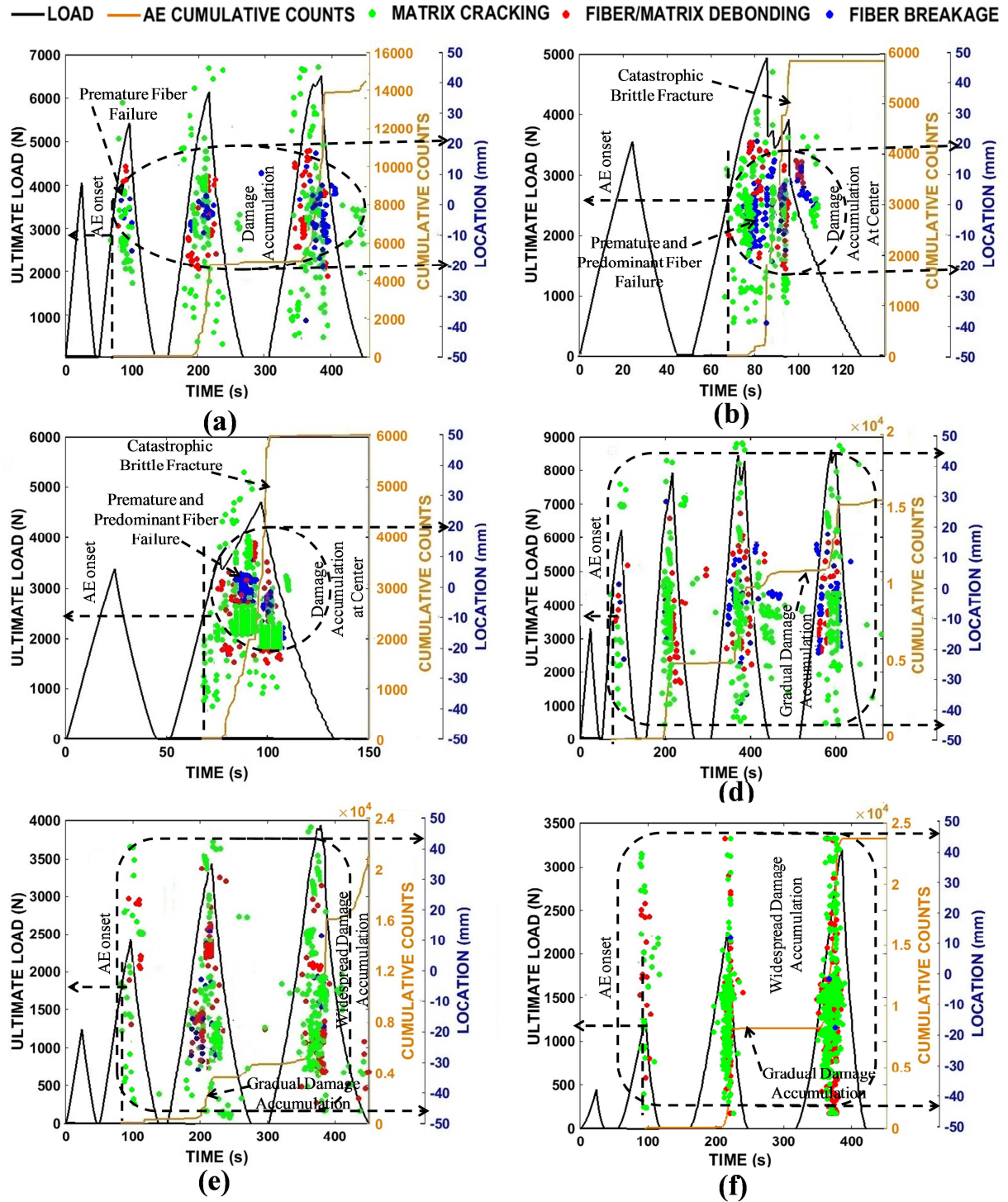


Figure 10: Indentation load, AE cumulative counts and AE event location versus time for (a) Virgin glass/epoxy specimen; dressed glass/epoxy specimens repaired using (b) 100G patches, (c) 75G25K patches, (d) 50G50K patches, (e) 25G75K patches, (f) 100K patches.

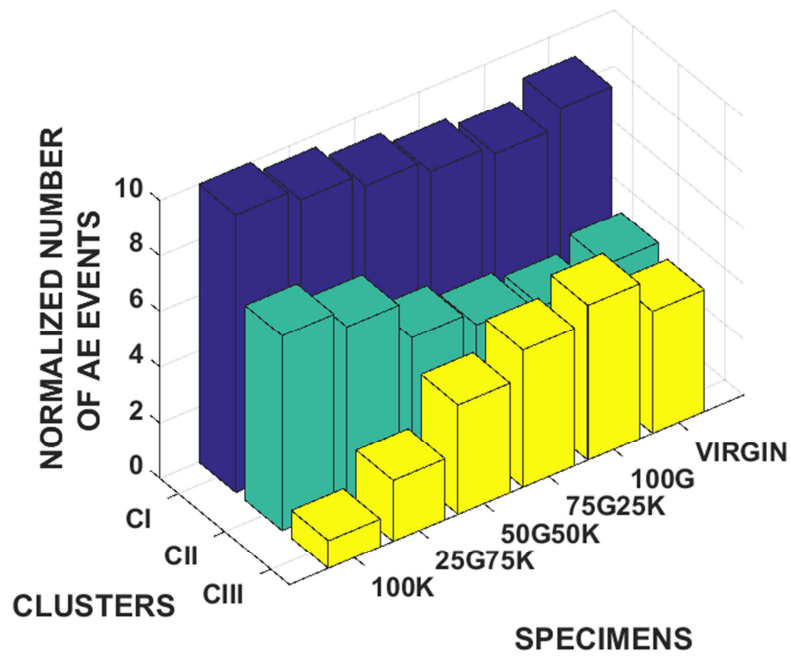


Figure 11: Normalized number of AE events (%) versus clusters for virgin and different repaired glass/epoxy specimens.